

1 Rapid response of fly populations to gene dosage across 2 development and generations

3

4 **Authors:** Xueying C. Li^{1,*#}, Lautaro Gandara¹, Måns Ekelöf¹, Kerstin Richter¹, Theodore
5 Alexandrov^{1,2,3}, and Justin Crocker^{1,*}

6 ¹ European Molecular Biology Laboratory (EMBL), Heidelberg, Germany

7 ² Molecular Medicine Partnership Unit between EMBL and Heidelberg University, Heidelberg, Germany

8 ³ BioInnovation Institute, Copenhagen, Denmark

9 [#] Present address: College of Life Sciences, Beijing Normal University, Beijing, China

10 * Corresponding authors: X.C.L., lixueying@bnu.edu.cn, J.C., justin.crocker@embl.de

11

12

13 *“The world was to me a secret which I desired to divine.”*

14 — Mary Shelley, *Frankenstein*

15

16 **Abstract:**

17 Although the effects of genetic and environmental perturbations on multicellular organisms are
18 rarely restricted to single phenotypic layers, our current understanding of how developmental
19 programs react to these challenges at a systems level remains limited. Here, we have examined
20 the phenotypic consequences of disturbing the classic *bicoid* network in *Drosophila*, which is
21 essential for anterior-posterior patterning in the early embryo. This network can be synthetically
22 perturbed by increasing the dosage of *bicoid*, which causes a posterior shift of the network’s
23 regulatory outputs and a decrease in fitness. To directly monitor network changes across
24 populations and time with extra copies of *bicoid*, we performed genome-wide EMS mutagenesis,
25 followed by experimental evolution. After only 8-15 generations, experimental populations have
26 normalized patterns of gene expression and increased survival. Using a phenomics approach, we
27 find that populations were normalized through rapid increases in embryo size driven by maternal
28 changes in metabolism and ovariole development. We extend our results to additional
29 populations of flies, demonstrating predictability. Together, our results necessitate a broader
30 view of regulatory network evolution at the systems level. In the future, such synthetic evolution
31 approaches using animal models could provide a generalizable platform for studying the
32 propagation of genetic perturbations across the many layers of complex multicellular systems.

33 **Introduction**

34 Changes in gene regulation underlie much of phenotypic evolution¹. However, our
35 understanding of regulatory evolution is likely biased², as most evidence is derived from
36 observations of sparse natural variation or limited experimental perturbations³, especially in a
37 developmental context. Furthermore, developmental networks orchestrate multiple processes that
38 span a range of organizational scales—from single cells to tissues and organs and to entire
39 organisms⁴. These complex regulatory programs also integrate metabolic states⁵ and
40 environmental cues in response to complex ecologies^{6,7}. However, developmental networks are
41 often explored using a reductionist approach, focusing on particular time windows or pathways
42 of development⁸. While such approaches have been foundational to our understanding of
43 development, this narrow focus may have limited our understanding of other ‘possible’ paths of
44 regulatory evolution that are not taken in nature⁹. A more unbiased view might teach us about the
45 constraints that govern evolutionary trajectories.

46 Quantitative genomics further challenges our models of how regulatory networks
47 function—for complex traits, most of the heritability is likely due to a large number of variants,
48 each with a small effect size¹⁰. Thousands of individual genes may contribute to phenotypes
49 through expression in relevant cells¹⁰, and the contributions of each genetic variant to
50 developmental fates are often small and challenging to measure^{11–13}. Therefore, it is essential to
51 consider regulatory evolution and development both at the systems level and across
52 populations^{14–16}. Clearly, approaches to elicit the relationships between different phenotypic
53 layers and how these changes manifest across populations are needed to understand the evolution
54 of developmental regulatory networks.

55 In this study, we explored the well-characterized early embryonic segmentation network
56 in *Drosophila*¹⁷ in response to extra copies of *bicoid*, a key morphogen in *Drosophila* embryonic
57 development. We were able to directly monitor developmental changes that rescue or mitigate
58 the phenotypic defects caused by altered gene expression and, in some cases, to even generate
59 novel phenotypes. We found that compensatory changes for developmental perturbation can
60 appear rapidly in the lab, with extensive phenotypic changes in gene expression, metabolism, and
61 maternal anatomical features. Finally, we suggest that patterns observed in laboratory evolution
62 can recapitulate phenotypic diversity in nature.

63

64 **Rapid population responses to extra copies of *bicoid***

65 The *bicoid* network in *Drosophila melanogaster* is one of the best-understood
66 developmental networks¹⁸. Bicoid is a transcription factor, the mRNA of which is maternally
67 deposited at the anterior of the egg and forms a concentration gradient along the anterior-
68 posterior (A-P) axis in the early embryo (**Fig. 1a-b, Supplemental Data File 1**). The gradient
69 provides positional information for downstream target genes, such as *hunchback* (*hb*), *giant* (*gt*),
70 *Kruppel* (*Kr*), and *even-skipped* (*eve*). These genes and others together constitute a complex
71 network that determines segmentation¹⁹ and scaling^{20,21} along the A-P axis of the embryo. The
72 network directly responds to the gene dosage of *bicoid*. In embryos with two extra copies of
73 *bicoid* (4*xbcd*, **Fig. 1a-c**), the cephalic furrow shifts toward the posterior¹⁹, indicated by the
74 expression of *eve*, an essential segmentation gene expressed in a striped pattern (**Fig. 1d-e**).
75 Despite the positional defects, the 4*xbcd* embryos can develop into normal adults—albeit with an
76 increased frequency of cuticle defects (**Fig. 1f-h**) and reduced viability to adulthood^{22,23} (68.5%,
77 **Fig. 1i, Table S1**).

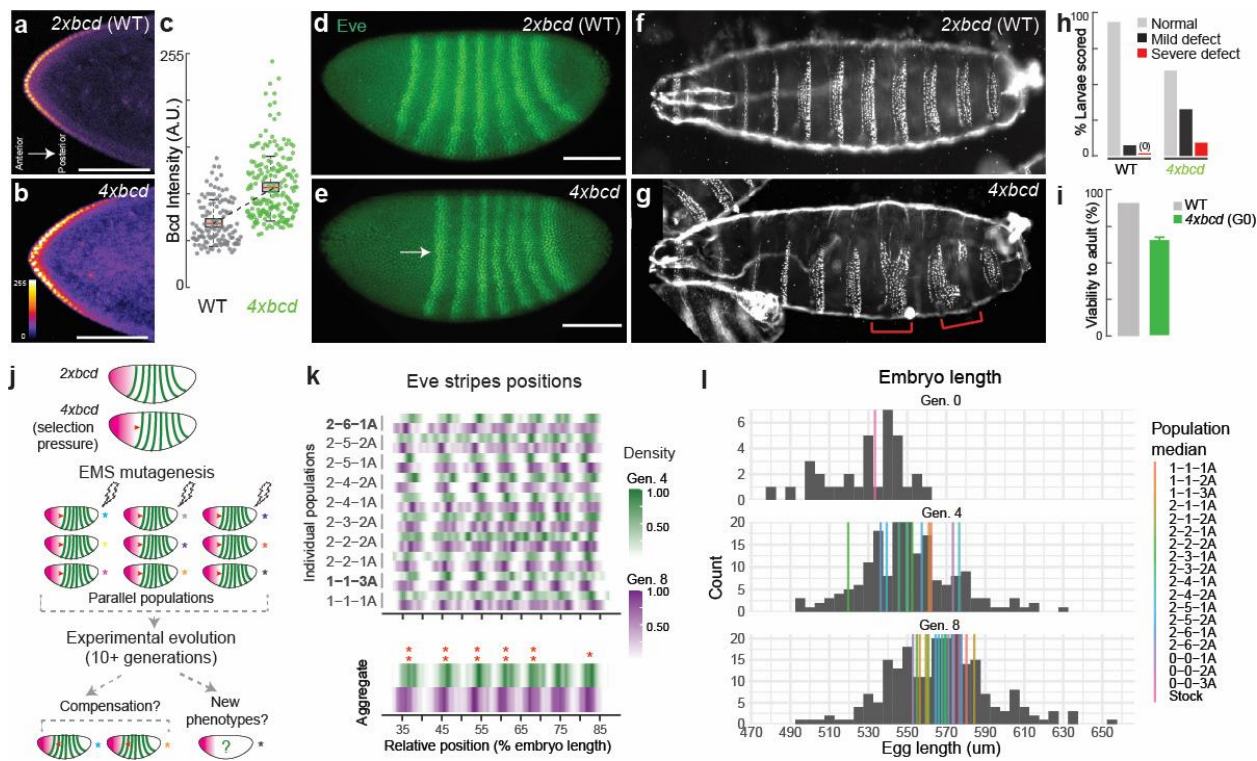
78 The reduced viability of 4*xbcd* flies is a fitness disadvantage that can be a selection
79 pressure in experimental evolution (**Fig. 1j**). To explore the system's capacity to respond to a
80 perturbation of Bicoid levels, we established 15 parallel laboratory populations from 7 pools of
81 chemically mutagenized 4*xbcd* flies (including replicates, see **Fig. S1**), along with three non-
82 mutagenized populations which represent the standing variation in the lab stock. Based on
83 whole-genome sequencing data, we estimated that the chemical mutagenesis with Ethyl
84 methanesulfonate (EMS) introduced, on average, 2.7 point mutations per Mb. Thus, we
85 estimated that the founding populations contained 1.7 million novel mutations (see **Methods**,
86 **Fig. S1c**), providing genetic diversity for selection. We set the 4th generation after mutagenesis
87 as our starting point of experimental evolution, assuming that the generally deleterious mutations
88 were purged in the first three generations. The mutagenized populations were maintained over
89 generations to select for compensatory mutations that can rescue or mitigate the fitness defect.
90 We primarily used *eve* stripe positions as an indicator for compensatory changes: the
91 compensated embryos should show *eve* stripes positions shifted to the anterior of the ancestral
92 4*xbcd* line [$37.2 \pm 0.4\%$ egg length (EL) for the first *eve* stripe, 95% confidence interval,
93 Generation 4] and closer to the wild-type positions ($28.3 \pm 0.6\%$ EL for the first stripe, VK33).

94 We found that compensation for the higher *bicoid* dosage occurred rapidly in our
95 experimental populations. From the 4th to the 8th generation, the first *eve* stripe shifted to the
96 anterior (toward the wild-type position) on average by 1.1% EL, from $37.2 \pm 0.4\%$ EL to $36.1 \pm$
97 0.2% EL ($p < 0.01$, Wilcoxon test) (all populations aggregated, **Fig. 1k, bottom panel**). Other
98 stripes also showed different magnitudes of anterior shifts compared to Generation 4, ranging
99 from 0.4% EL (stripe 7, $p = 0.04$, Wilcoxon test) to 1.0% EL (stripe 3 and 4, $p < 0.01$, Wilcoxon
100 test) (**Fig. 1k, bottom panel**). Among these populations, there were heterogeneous responses in
101 *eve* positions (**Fig. 1k, top panel**), with populations 1-1-3A and 2-6-1A showing significant
102 compensatory shifts in more than one stripe in Generation 8 (**Fig. 1k, Fig. S2a**). Other
103 populations showed different levels of shifts in *eve* stripes ranging from -2% EL to +2% EL (**Fig.**
104 **S2a**), but the statistical power in detecting these shifts was low due to a limited sample size. We
105 did not find a higher similarity between replicate populations from the same mutant pool than
106 those from different pools. Interestingly, the compensatory shifts in population 1-1-3A occurred
107 through a shortened anterior region, whereas population 2-6-1A compensated via an expansion
108 in the posterior region, suggesting multiple possible mechanisms for compensation (**Fig. S2b-f**).
109 These shifts could not be explained by deactivation of *bicoid* copies because the *eve* positions in
110 the evolved embryos were still much closer to those in the 4 \times *bcd* ancestors than in 2 \times *bcd*.
111 Despite the seemingly subtle compensatory shifts, we note that a shift of 1% EL was the highest
112 level of natural variation ever reported in *D. melanogaster*²⁴, suggesting that the early embryonic
113 segmentation network can shift rapidly in the lab under directed selection. In addition, the
114 experimental populations showed increased survival rates to eclosure after 16 generations ($74.2 \pm$
115 2.5%, averaged across all populations) compared to the ancestral line ($66.3 \pm 3.4\%$), consistent
116 with adaptation (**Fig. S1d**).

117 Unexpectedly, we found that compensation in the *bicoid* network coincided with an
118 increase in egg length across the populations. From the 4th to the 8th generation, median embryo
119 length increased from 550 um to 567 um (all populations aggregated, **Fig. 1l**, histogram, $p =$
120 1.81e-09, Wilcoxon test). Strikingly, despite variable embryo sizes, nine out of 12 populations
121 showed an increase in median embryo length (1-1-1A, 2-2-1A, 2-2-2A, 2-3-1A, 2-3-2A, 2-4-1A,
122 2-5-1A, 2-5-2A, and 2-6-1A; **Fig. 1l**, colored lines) and three of them (2-2-2A, 2-5-1A, 2-6-1A)
123 were statistically significant ($p < 0.05$, Wilcoxon test; **Fig. S2c**). This recurrent pattern suggests
124 that an increase in embryo length might provide a quickly accessible mechanism to buffer the

125 developmental stress caused by overexpression of *bicoid* and thus could drive the rapid
126 compensatory changes we observed.

127 In parallel to phenotypic changes, we also found recurrent directional changes at the
128 genomic level consistent with selection (**Fig. S3**). We performed low-coverage whole-genome
129 sequencing for all 18 populations at the 3rd and 7th generation and focused on changes in allele
130 frequency in common variants shared across populations (i.e. standing variation) to understand
131 the population dynamics at a broad scale. We found 16,394 biallelic variants showing consistent
132 increases or decreases in allele frequency in two or more populations (Fisher's exact test, FDR-
133 adjusted $p < 0.05$, **Supplemental Data File 2**). Based on a sign test, 181 of them were biased
134 toward being maintained or purged in six or more populations (**Fig. S3c**). Recurrent gain or loss
135 of these alleles across multiple populations could suggest selection. For example, a non-
136 synonymous mutation in Melted (F21V) was purged in six populations at the 7th generation (**Fig.**
137 **S3d**), which could be beneficial because *melted* was linked to growth and metabolic pathways,
138 and its mutant showed nutrient deprivation²⁵. Other variants potentially under directed selection
139 include those related to metabolism (e.g. *Apolip*, **Supplemental Data File 2**) and ovariole
140 development (e.g. *mtgo*, *bru3*, **Fig. S3d, Supplemental Data File 2**)²⁶. These changes in allele
141 frequency are consistent with rapid adaptation in the laboratory populations, with possible links
142 to maternal and metabolic-related genes.



143

144

Fig. 1. Rapid changes of the *bicoid* network after experimental perturbation.

(a, b) Bicoid gradient along the anterior-posterior axis in embryos with two (wild-type) or four copies of *bicoid* (anti-Bicoid immunostaining, stage 4 embryos). Scale bar = 100 um.). (c) Bicoid levels in the ten most anterior nuclei, quantified across 11 and 12 embryos for wild-type and 4 \times *bcd*, respectively. (d, e) Expression of *even-skipped* (*eve*) (anti-*Eve* immunostaining, stage 5 embryos). Scale bar = 100 um. (f, g, h) Cuticle phenotypes, with red brackets in (g) highlighting severe defects. (i) Viability to adulthood, with the error bar in G0 representing the standard error of three measurements. (j) Scheme of experimental evolution. (k) Distribution of *eve* stripe positions in mid-stage 5 embryos, detected by *in situ* hybridization. Top, individual populations. Bottom, all populations aggregated (N=60 for Generation 4, N=217 for Generation 8). Intensity represents the scaled density of the designated population. Asterisks indicate shifts in the scaled position between generations. **, p < 0.01; *, p < 0.05 (Wilcoxon test, FDR-adjusted). (l) Distribution of embryo length across generations (grey histogram, all populations aggregated; N=34 for Generation 0, 176 for Generation 4, 217 for Generation 8). Color bars represent the median of each population. Population 0-0-1A, 0-0-2A, and 0-0-3A are non-mutagenized populations representing standing variation in the lab stock. G0 in (i) and (l) represents a non-mutagenized 4 \times *bcd* stock. All boxplots in this work are defined as follows: center line, median; box limits, the first and third quartiles; whiskers, 1.5x interquartile range.

145

146

Compensation of *bicoid* overexpression through an increase in embryo length

147

To further address the possible link between embryo size and the *bicoid* network, we

148

focused on population 2-6-1A to dissect the developmental changes before and after laboratory

149

evolution. In this line, *eve* stripes consistently shifted to the anterior in the 8th and the 10th

150

generation compared to the 4th generation (Fig. 2a-c; Fig. S4a), with the shift of the last stripe

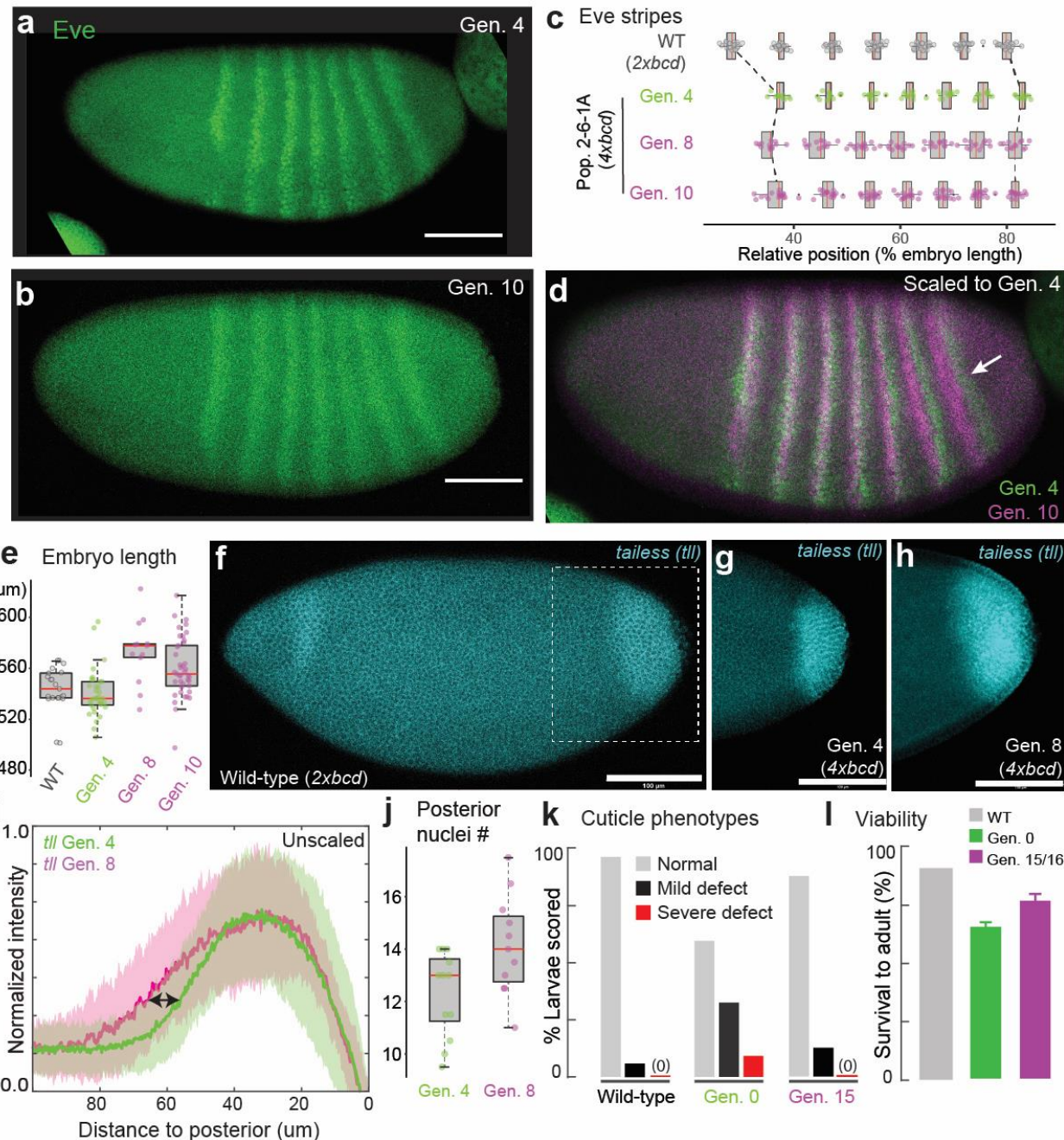
151

being the most prominent (Fig. 2c-d). We found that the shifts occurred simultaneously with an

152 expansion of the posterior region: the egg length was consistently longer in both generations
153 (540.5 ± 6.5 um at Generation 4, 573.5 ± 13.6 um at Generation 8, and 560.4 ± 7.1 um at
154 Generation 10; **Fig. 2e, Fig. S4b**). The expression of *tailless*, a gap gene that specifies the
155 posterior identity, was also wider in the 8th generation than the 4th generation (**Fig. 2f-i**). While
156 the total number of nuclei along the A-P axis has not significantly changed (**Fig. S4c**), consistent
157 with early embryos' limited capacity to regulate cell number²⁷, there was a slight increase in the
158 number of nuclei in the posterior region, from *eve* stripe 7 to the posterior pole at Generation 8
159 (12.3 ± 0.9 vs. 14.1 ± 1.1 , $p = 0.048$, Wilcoxon test, **Fig. 2j**), as well as an overall increase in the
160 distance between nuclei (6.39 ± 0.23 um vs. 6.82 ± 0.13 um, $p = 0.004$, Wilcoxon test, **Fig. S4d-e**). Consistent with compensatory changes, the line has stabilized phenotypes across phenotypic
161 scales, including cuticle phenotypes (**Fig. 2k**) and viability to adulthood after 15-16 generations
162 (**Fig. 2l**).

164 The compensation via embryo size appeared to be relatively short-term, because the
165 embryo length of population 2-6-1A peaked at Generation 8 and 10, but gradually reduced after
166 Generation 15 and resumed wild-type level at Generation 49 (**Fig. S4a-b**). This could be due to
167 the fact that overly large embryos might have deleterious effects and cannot persist as a long-
168 term solution in the standard environmental conditions employed in this work. Such a turnover in
169 adaptive strategies is not uncommon in evolution²⁸⁻³¹. Future research along these lines could
170 reveal alternative strategies to compensate for high *bicoid* dosage that is independent of embryo
171 size, such as the response of Population 1-1-3A, which showed a shortened anterior region (**Fig.**
172 **1k, Fig. S2**).

173 Together, these data lead us to hypothesize that the compression of the trunk and tail
174 caused by extra Bicoid might be mitigated in larger embryos due to more space in the posterior
175 region. These results are consistent with previous findings on the interaction between egg size
176 and the *bicoid* network^{24,32,33}. Furthermore, because egg size is a highly polygenic and evolvable
177 trait³⁴⁻³⁶, it might have provided a large capacity to respond rapidly to genetic and environmental
178 changes.



179

Fig. 2. Compensatory changes in gene expression, embryo length, cuticle, and viability.

(a-d) Eve stripes in Population 2-6-1A (anti-Eve staining), with the arrow in (d) showing a prominent anterior shift in the 7th stripe. The shifts were quantified in (c) from *in situ* data (eve co-stained with *sna*). (e) Increases in embryo length at the 8th and 10th generation. (f – i) *tailless (tll)* expression, detected by *in situ* hybridization. (i) shows the normalized intensity profiles aligned at the posterior end. Solid lines are average *tll* intensity and the shaded panels denote the standard deviation. N = 22 and 14 for the 4th and the 8th generation, respectively. (j) The number of nuclei from the posterior boundary of eve stripe 7 to the posterior pole. (k) Rescue of cuticle defects. (l) Viability to adult, with error bars representing the standard error of three measurements (also see Fig. S1). Scale bar = 100 um. G0 in (k) and (l) represents a non-mutagenized 4 \times bcd stock.

180

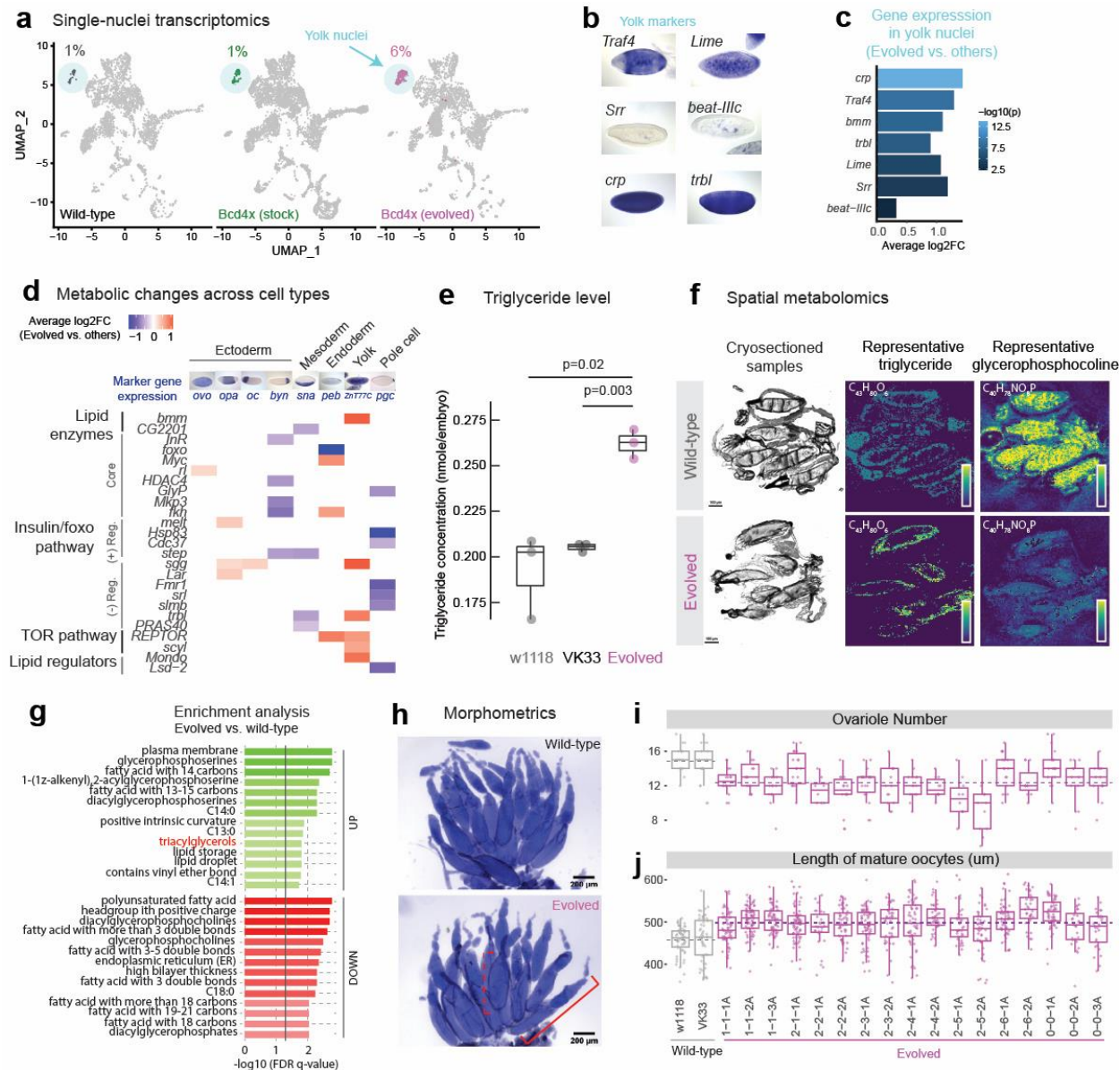
181 **Multi-modal analysis reveals changes in metabolism and ovariole development**

182 To identify possible molecular bases that can support the rapid phenotypic stabilization
183 through changes in egg length, we performed single-nuclei transcriptomics with early embryos in
184 the evolved line (2-6-1A, Generation 20) (**Fig. S5, Table S2**). The evolved line had a striking
185 increase in the proportion of yolk nuclei compared to wild-type or the 4 $xbcd$ lab stock (6% vs.
186 1%, $p < 0.001$, fisher's exact test, **Fig. 3a**), consistent with the increased nutritional need of
187 larger embryos. Among marker genes of the yolk cluster, there were 230 genes differentially
188 expressed in the evolved line, including those related to metabolism (*bmm*, *trbl*, *Lime*, *Srr*) and
189 cell growth (*crp*, *Traf4*) (**Fig. 3b-c**, and **Supplemental Data File 3**). Previous research suggests
190 that the *Drosophila* body/organ size can be directly controlled by signaling pathways involved in
191 metabolic regulation and cell growth, such as the insulin signaling pathway^{37,38}. We found a
192 number of metabolic genes differentially expressed in the evolved line across multiple cell types,
193 including epidermal ('*ovo*'), trunk ('*opa*'), anterior ('*oc*') and posterior ('*byn*') clusters in the
194 ectoderm, as well as in mesoderm, endoderm, yolk and pole cells (**Fig. 3d, Supplemental Data**
195 **File 4**).

196 The changes in yolk content and gene expression might imply a broader change in
197 maternal metabolism to direct more nutrients into the eggs, and thus enable larger embryo sizes.
198 Indeed, we found that the evolved embryos contained more triglycerides (TG) than two wild-
199 type lines (**Fig. 3e**). Triglycerides are essential components of yolk-related lipid droplets³⁹ that
200 can act as metabolic fuel for *Drosophila* embryogenesis⁴⁰, and high triglyceride levels have been
201 linked to bigger embryo size in multiple animals^{41,42}. To further characterize this metabolic
202 alteration, we performed MALDI-imaging mass spectrometry (MALDI-IMS) in positive ion
203 mode⁴³ on cryo-sectioned slices of ovaries. This technique allowed us to reconstruct entire mass
204 spectra for single oocytes, and thus trace this phenomenon back to the oocyte stage. We found
205 differences in the lipid signature of oocytes between the evolved 4 $xbcd$ line (2-6-1A, Generation
206 42) and wild-type (w1118) (**Fig. S6a**), including elevated levels of triglycerides and decreased
207 levels of glycerophosphocholines in the evolved line (**Fig. 3f-g, Fig. S6b-c**). Additionally, there
208 were global differences in the fatty acid (FA) distribution in the evolved line, showing a higher
209 abundance of FAs with 13, 14, and 15 carbons, and reduced levels of FAs with 18 carbons on
210 their chain (**Fig. 3g**). This observation was confirmed by tandem mass spectrometry coupled
211 with MALDI-IMS in negative ion mode, which independently detects a wide range of lipid ions

212 (Fig. S6d-f; also see Methods). Overall, these results show that the line has altered its lipid
213 metabolism in a way that is consistent with bigger embryo sizes and higher energy requirements.

214 The changes in gene expression and lipid composition suggest rapid physiological
215 changes at the maternal level. We examined the ovaries of the experimental populations and
216 found that they tended to have fewer ovarioles (12.4 ± 0.3 vs. 14.8 ± 0.7 , all populations
217 aggregated vs. wild-type aggregated, same below) and longer oocytes (498.4 ± 2.9 um vs. 458.0
218 ± 8.2 um) than wild-type lines (Fig. 3h-j), consistent with a previous report that the egg size
219 difference between *Drosophila* lines originated from oogenesis⁴⁴. Therefore, the compensation
220 could occur through a trade-off between ovariole number and oocyte size⁴⁵, possibly through
221 growth-related mechanisms such as the insulin pathway^{34,46}. Furthermore, we found that the
222 change in size was specific to oogenesis and likely to have metabolic rather than behavioral
223 underpinnings because we did not observe significant differences in larval length or larval
224 feeding behavior (Fig. S7) ³⁶.



225

Fig. 3. Phenotypic changes in gene expression, metabolism and ovariole development in the evolved lines. (a) UMAP of single-nuclei transcriptomes of stage 5 embryos (see Fig. S6 for details). The colored clusters show yolk nuclei. Wild-type is VK33. The evolved line is population 2-6-1A at Generation 20. **(b)** Representative marker genes of yolk nuclei. **(c)** Representative marker genes of yolk nuclei that were differentially expressed in the evolved line. **(d)** Changes in expression of metabolic genes across cell types between the evolved line and the other two samples. Only significant changes (adjusted p-value < 0.05) are shown. (+) Reg., positive regulators; (-) Reg., negative regulators. FC, fold change. Images of marker gene expression in **(b)** and **(d)** are from BDGP *in situ* database⁴⁷. **(e)** Enzymatic determination of triglyceride levels in stage 5 embryos (Generation 50 for population 2-6-1A). Points represent values from independent homogenates made from 50 embryos each. P values are from Student's t-test. **(f)** MALDI-IMS of ovaries. Left, middle sections from ovaries employed in MALDI-IMS. Scale bar = 100 μ m. Middle, spatial distribution of a representative triglyceride, TG(40:1) at m/z=715.5846 normalized by another triglyceride which showed constant levels across all experiments (TG(44:3) at m/z=767.6159). Right, spatial distribution of a representative glycerophosphocholine, PC(32:1) at m/z=732.5537, in the sectioned ovaries. The evolved line is 2-6-1A from Generation 42. **(g)** Enrichment analysis comparing oocytes from the 2-6-1A and w1118 lines, based on the abundance values for 122 lipids detected through MALDI-IMS (same experiments as **f**). The vertical solid line indicates a cutoff at FDR q-value of 0.05. Triacylglycerols were highlighted in red. **(h)** Ovaries

of wild-type (w1118) and evolved (2-6-1A, Generation 39) lines, stained with DAPI. The solid red bracket indicates an ovariole, and the dashed red bracket indicates a mature oocyte. Scale bar = 200 um. (i) Ovariole number and (j) length of mature oocytes of wild-type and the evolved lines (Generation 39). The horizontal dashed lines represent the mean of all wild-type/evolved lines aggregated ($p = 9.783e-09$ for ovariole number and $p < 2.2e-16$ for oocyte length, Wilcoxon test).

226

227 **Laboratory experiments are consistent with phenotypes from additional fly lines**

228 Embryo size is known to vary widely within and between *Drosophila* species²⁴ and
229 across environments³⁵. As such, changes in embryo size could provide a way to rapidly mitigate
230 the effects of Bicoid dose. To test if our observations could be extended, we examined two
231 inbred lines isolated from the wild, Ind and Canton-S, with the former having larger embryos
232 than the latter²⁴ (**Fig. 4a**). The anterior Bicoid concentration was also higher in the larger Ind
233 embryos (**Fig. 4b-c**), consistent with the relationship between Bicoid and embryo size in our
234 laboratory-evolved lines, as well as previous results^{44,48-50}. These two natural isolates also show
235 differences in ovariole number and oocyte length (**Fig. 4d**), as well as the level of triglycerides
236 (**Fig. 4e**). Collectively, these observations suggest that the coupling among the *bicoid* network,
237 egg size, maternal physiology, and metabolism could also exist in nature.

238 Next, to test if the bigger embryo size of the Ind genetic background could relieve the
239 stress on the developmental network elicited by Bicoid overexpression, we crossed the *bicoid*
240 transgenes into these inbred lines. In the crosses, the F1 offspring have 50% of genetic
241 information from the wild isolates and have two extra copies of *bicoid* inserted on the second and
242 the third chromosomes, respectively (4 $xbcd$ in total, see **Fig. S8a** for the crossing scheme). We
243 also crossed them to a wild-type lab strain (VK33) to control for background effects. We found
244 that embryos from F1 individuals in Ind/lab background were larger than those in Canton-S/lab
245 background (**Fig. S8b**), suggesting that the Ind background had a dominant effect on embryo
246 size. The *eve* stripes in Ind/lab background were located further to the anterior than the Canton-
247 S/lab background in the control crosses (2 $xbcd$) (**Fig. S8c**), suggesting natural variation in the
248 capacity for scaling of the network. Such variation might be in favor of buffering stresses such as
249 overexpression of *bicoid* - the difference was also present in embryos with 4 $xbcd$, with the *eve*
250 stripes of Ind embryos being anterior to those of Canton-S embryos, i.e. closer to the wild-type
251 positions (**Fig. 4f-i**). Interestingly, the positions of *eve* stripes (**Fig. 4i**) and cuticle phenotypes
252 (**Fig. 4j-l**) of 4 $xbcd$ -Ind embryos resembled those of population 2-6-1A. 4 $xbcd$ embryos in the
253 Ind background also had higher viability to adulthood compared with those in Canton-S or lab

254 background (**Fig. S8d**), consistent with a higher tolerance of *bicoid* overexpression in larger
 255 embryos. Together, the evolved line is similar to Ind across a number of key phenotypes,
 256 supporting the hypothesis that changes in maternal contributions to embryo sizes could be used
 257 to buffer the dosage of *bicoid*.

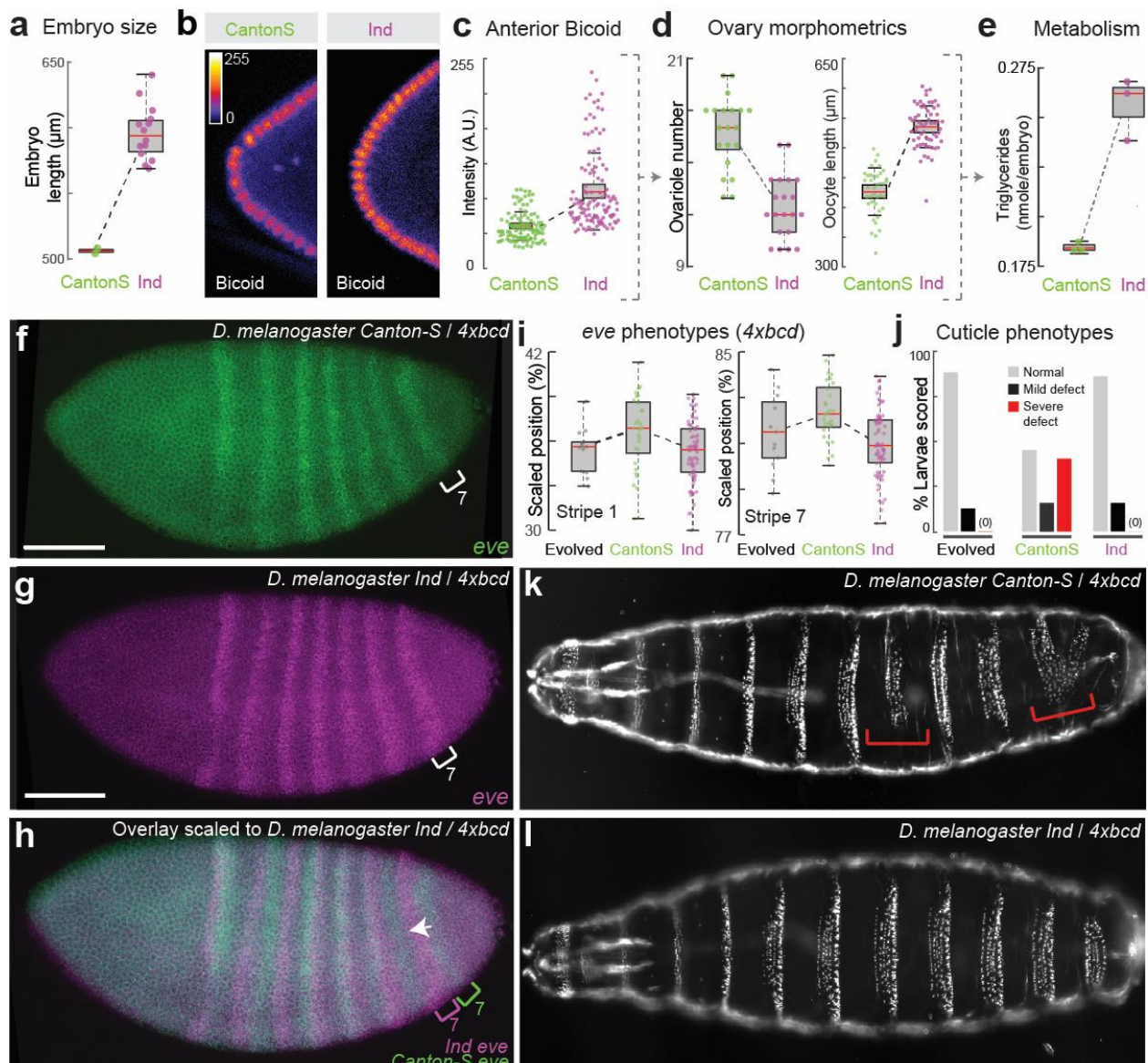
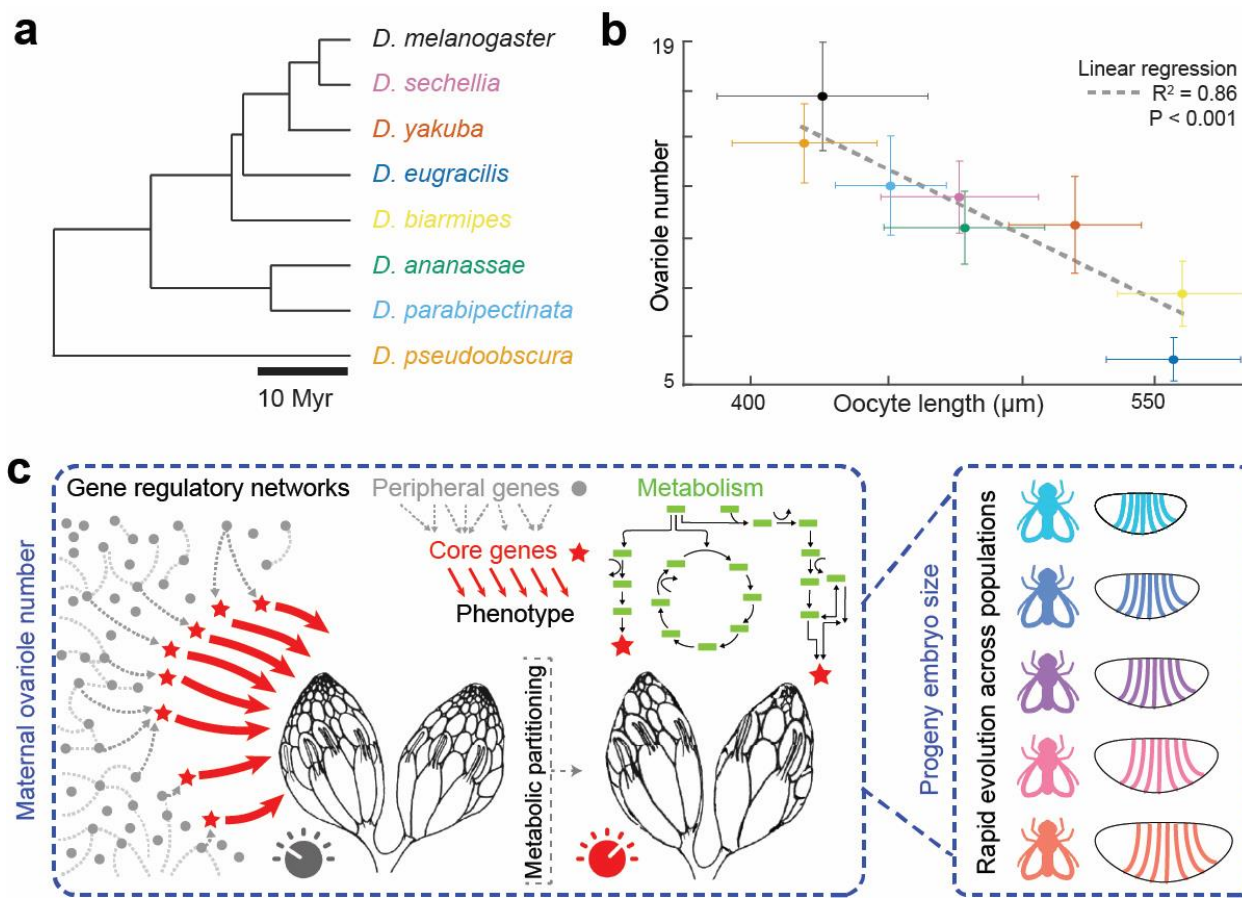


Fig. 4. Wild populations' responses to extra copies of *bicoid* and model for adaptation.
(A) Embryo size and **(B-C)** anterior Bicoid concentration (anti-Bicoid staining) of Ind and Canton-S. Each point represents one nucleus in **(C)**, quantified across 18 and 10 embryos for Ind and Canton-S, respectively. **(D)** Ovariole number, oocyte length, and **(E)** level of triglycerides per embryo of Ind and Canton-S. **(F-I)** eve stripe positions and **(J-L)** cuticle phenotypes of Ind and Canton-S when carrying 4 \times bcd. Scale bar = 100 um. The red brackets in **(K)** highlight severe defects. Data for the evolved line in **(I)** were from Generation 8. See **Fig. S8** for full data.

259

260 The trends we found from experimental evolution, genetic perturbations, and the findings
261 from the larger *D. melanogaster* *Ind* line, are all in line with evidence that *Drosophila* can adapt
262 rapidly to laboratory culture on ecological timescales⁵¹. To explore the broader context of these
263 results, we looked across a number of closely related *Drosophila* species (Fig. 5a, Fig. S9),
264 testing the relationship between ovariole number and oocyte lengths (Fig. 5b). Consistent with
265 previous results^{36,45}, we see a strong correlation across the *Sophohora* subgenus indicating that
266 such a trait may be consistent across a broader evolutionary context.
267



268
269 **Fig. 5. Laboratory evolution predicts phenotypes of wild species.**
270 (a) Phylogeny of species tested⁵². (b) The relationship between ovariole number and oocyte length, error bars
271 denote the standard deviation; colors are indicated in (a). *D. melanogaster* was represented by Canton-S. (c)
272 Model for maternal compensatory changes in laboratory evolution [adapted from Liu et al. (2019)⁵³]. The
273 embryonic patterning network is connected to a broad gene regulatory network via core genes (red stars) involved
274 in maternal metabolism that tunes the size of ovarioles.

270

271 **Discussion**

272 Little is known about how organisms respond to developmental perturbations in short
273 timescales. The early segmentation network downstream of Bicoid has been characterized as a
274 highly dynamic⁵⁴ yet robust network to ensure precise scaling of gap gene boundaries^{21,24,48,55}.
275 Perturbations to the network, such as a change in *bicoid* dosage, can lead to substantial
276 patterning defects and fitness disadvantages²² (**Fig. 1**). Leveraging the fitness disadvantage as a
277 selection pressure provided us an opportunity to examine the robustness and evolvability of
278 developmental systems. We found compensatory phenotypic changes within 8-15 generations,
279 reflected in gene expression, larval morphologies, and survival to adulthood (**Figs. 1-2**). These
280 results are consistent with the recent findings that adaptation in *Drosophila* was evident over
281 only one to four generations in response to environmental changes, including changes in egg-
282 size⁵¹. Such rapid phenotypic adaptation and large allele-frequency shifts over many independent
283 loci in response to developmental changes may be a common mechanism for gene-regulatory
284 network evolution⁵¹.

285 One prominent phenotypic response to extra copies of *bicoid* was a general increase in
286 egg length (**Figs. 1l & 2e**). What could be the mechanism for the large embryos to ameliorate the
287 fitness defect caused by 4*bcd*? One possibility is that the enlarged posterior region relieved
288 some of the compression in the abdominal region, which has been associated with lack of cell
289 death²². The observed change in the posterior was also consistent with a recent study showing
290 that posterior boundaries in *Drosophila* embryos are highly dynamic and sensitive to gene
291 dosage⁵⁶. Furthermore, the compensation could occur through altered distribution of important
292 factors in the segmentation network, which consists of maternal factors (*bcd, nos, tor*), gap genes
293 (*hb, gt, kni, Kr*) and pair-rule genes (*eve*, etc). Previous studies have shown that, when *bcd*
294 dosage changes over a fivefold range, the expression boundaries of downstream gap genes and
295 pair-rule genes change over a much smaller magnitude (up to 2-fold)⁵⁷, highlighting the
296 importance of additional maternal factors such as Nanos or Torso, as well as cross-regulation
297 among the gap genes themselves. Therefore, it would be of future interest to quantitatively
298 characterize the dynamics of these factors over generations to understand how the evolutionary
299 compensation occurred.

300 Additionally, understanding the compensatory mechanism for 4*bcd* would be promising
301 in revealing unknown properties of the segmentation network. In wild-type embryos, the gap
302 genes and pair-rule genes scale at 1% precision within a short developmental time window, using

303 an unscaled Bcd gradient as input^{58,59}. Theoretical models suggest that the information needed
304 for the precise scaling is sufficiently encoded in the above-mentioned factors⁶⁰. In this study, we
305 found a shift of 1.1% EL in *eve* stripe positions under 4 $xbcd$ selection, which seemingly
306 “escaped” the precise control of the network. This finding is in line with previous observations
307 that embryonic geometry can affect the scaling of gap gene boundaries under perturbations,
308 including genetic manipulation³² and artificial selection^{33,48,50}. Given further molecular
309 characterization, these perturbed systems have the potential to provide new models for network
310 dynamics, incorporating the interactions between the embryonic size-control network and the
311 segmentation network^{44,49,50}.

312 The rapid phenotypic compensation driven by embryo size is likely related to its genetic
313 architecture. Egg size is a trait known to be both highly polygenic³⁴ and evolvable in both
314 common garden experiments^{33,51} as well as across natural populations^{24,35,36}. As such, the egg-
315 size network might provide a much larger set of targets for selection than targets directly
316 downstream of Bicoid, and hence the change in egg length appeared as the first response in a
317 short evolutionary timescale. These results are consistent with models that posit that phenotypic
318 evolution may be driven by many loci of small effect^{61,62}. Furthermore, the rapid changes were
319 associated with changes in ovariole number, which is also known to be controlled by many
320 genes²⁶, resulting in changes in metabolism and embryo size. Therefore, there could be numerous
321 genes at different phenotypic levels that provide evolutionary accessibility to compensation. It is
322 possible that the segmentation network, which can readily scale within and between species²¹, is
323 the result of selection for a highly evolvable system that provides developmental plasticity for
324 early embryos across variable ecologies⁶³ (**Fig. 5c**).

325 Our study is subject to a few limitations, highlighting the challenges in longitudinal
326 studies of laboratory populations. In our experimental-evolution design, we set up multiple
327 parallel-evolving populations with an intensive sampling schedule with the aim to characterize
328 network dynamics at scale. However, despite our efforts in high-throughput embryo-handling
329 and automated imaging^{2,64}, we were often limited by technical factors such as sample size, batch
330 effects, and drift. A higher level of automation would allow systematic examinations of different
331 adaptive strategies in parallel populations (e.g., compensatory mechanisms other than embryo
332 size) and exploration of the generalizability of the proposed model. One of the challenges is that
333 random mutagenesis introduces many mutations that may be both unrelated and highly

334 deleterious⁶⁵. Further, mapping causal variants, which can be broadly distributed with low-effect
335 sizes, remains a challenge⁶⁶. Therefore, in the future, more targeted *in vivo* mutagenesis
336 approaches biased towards gene regulatory networks can be developed for the study of the
337 genetics and evolution of the *Drosophila* regulatory genome.

338 The phenotypic differences were not limited to early embryonic development but
339 included changes in lipid metabolism (not only increased yolk content and triglyceride levels, but
340 also changes in the relative abundance of physiologically relevant phospholipids), cell-type-
341 specific gene expression (rewiring of metabolic gene network), and maternal anatomy (reduced
342 ovariole numbers) (Fig. 3). These results show that perturbation of one node of the
343 developmental network, the *bicoid* dosage, can lead to profound organism-wide responses across
344 multiple phenotypic scales. Importantly, these observations highlight the deep connections
345 between multiple phenotypic layers of multicellular systems and argue for a broader ‘phenomics’
346 perspective¹⁶, instead of a strictly gene-centric view. Exploring the interplay of metabolic and
347 developmental networks could transform our understanding of evolution and development across
348 variable ecologies^{5,15}, as such processes are fundamentally linked⁶⁷. In the future,
349 synthetic evolution approaches using animal systems could provide a generalizable platform for
350 the dissection of gene regulation and complex genomes.

351

352 **Methods**

353 **Fly genetics**

354 The eGFP-Bicoid fusion construct was designed according to Gregor et al. (2007)⁶⁸ (see
355 **Supplemental data File 5** for the construct map). The construct was synthesized and cloned into
356 placZattB by Genscript, and was transformed into *D. melanogaster* at the VK18 or VK33
357 landing site following standard PhiC31 integrase protocol, with the help of injection service
358 provided by Alessandra Reversi at EMBL. The transformants at the VK33 site were
359 homozygosed by sibling crosses to construct a stable 4 \times *bcd* line and subsequently used in
360 mutagenesis and experimental evolution.

361 We also established balancer stocks from the transformants at VK18 (second
362 chromosome) and VK33 (third chromosome) sites, and used them to generate a 6 \times *bcd* line, with
363 an extra copy of *bicoid* on each of the second and the third chromosomes.

364 To examine the response to extra copies of *bicoid* in wild populations, virgins of Ind
365 (“Mysore” strain, old stock #3114.4 from National Drosophila Species Stock Center, US) and
366 Canton S (Bloomington stock #64349) were crossed to 6 \times *bcd* males. The F1 flies are
367 heterozygous for the alleles from the wild populations and carry two extra copies of *bicoid*. They
368 were used to set up egg-collection chambers and the F2 embryos were examined for *eve*
369 expression, cuticle phenotypes, and fitness (Fig. S8a). To control for background effects, the
370 natural isolates were crossed to the VK33 stock, which has the same background as the 6 \times *bcd*
371 line.

372 At Generation 40, we outcrossed 2-6-1A males to wild-type w1118 or VK33 for four
373 generations. In each generation, males with orange eyes (heterozygous for the *egfp-bicoid*
374 transgene) were crossed to virgins of w1118 or VK33. After four generations, males and virgins
375 with orange eyes were mated, and their progeny were selected for homozygotes (red eyes) to
376 create ‘new’ 4 \times *bcd* lines. In this way, we expect to remove or ‘dilute’ 2-6-1A-associated
377 mutations and study the effects of 4 \times *bcd* without any compensatory evolution.

378 The non-*melanogaster* species were a generous gift from Nicolas Gompel, with the
379 exceptions of *Drosophila parabipectinata* which was kindly provided by Artyom Kopp, and
380 *Drosophila virilis*, which was kindly provided by Eileen Furlong. Strain background: *D.*
381 *ananassae* (TSC 14024-0371.13), *D. biarmipes* (TSC 14023-0361.01), *D. eugracilis* (from the
382 US National *Drosophila* Species Stock Center), *D. parabipectinata* (inbred derivative of strain
383 TSC 14024-0401.02), *D. pseudoobscura* (TSC 14011-0121-94 USA), *D. sechellia* (TSC 14021-
384 0248-25), *D. yakuba* (TSC 14021-0261.01) and *D. virilis* (*w*⁻).

385

386 **Mutagenesis and experimental evolution**

387 EMS-mutagenesis was performed according to Bökel (2008)⁶⁹. Briefly, around 1,000
388 4 \times *bcd* male flies (G0) were fed with 1% sucrose solution containing 25mM EMS, and were then
389 mated to 4 \times *bcd* virgins. Around 3,500 F1 flies were used to establish 7 independent mutant
390 pools, with 400-600 flies per pool. Specifically, the mutagenesis was done in two batches: flies
391 from the first batch were used to establish one mutant pool, labeled 1-1, and flies from the
392 second batch were used to establish six mutant pools, labeled 2-1 to 2-6. Mutation rate did not
393 obviously differ between the two batches based on subsequent genomic analysis (see below).

394 Each mutant pool was used to seed 2-3 bottles of progenies consecutively ('set A') and
395 these bottles were replicated at the 3rd generation ('set B'), to provide 4-6 replicate populations in
396 total for each mutant pool (**Fig. S1a**). For example, Pool 1-1 was used as parents to produce
397 Populations 1-1-1A, 1-1-2A and 1-1-3A, by transferring the parents to a new bottle every 4-5
398 days. F3 flies from these populations were used as parents to produce Populations 1-1-1B, 1-1-
399 2B, and 1-1-3B, respectively. Populations in set B were primarily for backups in this study.

400 The flies were maintained at 25°C under standard fly-rearing condition under non-
401 overlapping generations, to select for rescuing mutations. The population size was approximately
402 200-500 for each generation. Three populations of non-mutagenized 4 \times bcd flies were maintained
403 under the same condition for comparison (labeled 0-0-1A, 0-0-2A and 0-0-3A). During the first
404 15 generations, the populations were sampled every 2-5 generations for embryo collection, and
405 the adult flies were frozen for genomic DNA (**Fig. S1b**).

406

407 **Embryo fixation, antibody staining and fluorescent *in situ* hybridization**

408 *Drosophila* embryos were fixed and stained following standard protocols⁷⁰. In particular,
409 stage-5 embryos were acquired from a 5-hr egg-laying window at room temperature. A fixation
410 time of 18 min was used for these embryos, to adapt to the sensitivity of Eve antibody. The Eve
411 antibody (mouse, Developmental Studies Hybridoma Bank, 2B8-concentrate) was used at 1:20
412 dilution. Bicoid antibody (rabbit) was a gift from Pinar Onal and Stephen Small, and was used at
413 1:250. DIG-, FITC- or biotin-labeled, antisense RNA-probes were used to detect gene expression
414 of *eve*, *sna*, or *tll*, respectively. All embryos were mounted in ProLong Gold with DAPI, and
415 imaged on a Zeiss LSM 880 confocal microscope, under 20x (air, 0.8 NA) or 25x (oil, 0.8 NA)
416 objective.

417

418 **Image analysis**

419 All images were rotated to orient along the A-P axis before analysis, with the A-P axis
420 positioned horizontally and the dorsal-ventral (D-V) axis positioned vertically (see **Fig. S2d** for
421 an example).

422 **Position of eve stripes.** Images from fluorescent *in situ* hybridization of *eve*, *snail* (*sna*) and
423 *tailless* (*tll*) were used to quantify *eve* position precisely. Embryos were imaged as Z-stacks, with
424 the measurements performed on the Z-slice where *eve* and *sna* were in focus. We manually

425 extracted the positions of the intersection of *sna* expression and the anterior boundary of each
426 *eve* stripe in mid-stage 5 embryos (see **Fig. S2d** for an example), staged based on the degree of
427 membrane invagination. The use of *sna* to mark a particular dorsal-ventral position on the *eve*
428 stripes enabled precise quantification of the *eve* positions, which could also explain the
429 differences between our results on Ind and Canton-S and a previous publication²⁴.

430 **Embryo length.** Embryo length was manually extracted from Z-stacked confocal images, from
431 anterior to posterior, excluding the pole cells.

432 **Bicoid concentration.** Bicoid intensities were acquired from anti-Bicoid staining by extracting
433 the average nuclear intensity for ten nuclei at the anterior pole for each embryo, as per Dubuis et
434 al. (2013)⁷¹.

435 **Tll profiles.** The intensity profiles were extracted from a rectangular region of 3-4 cells' height
436 along the A-P axis from max-projected confocal images⁷², normalized to peak intensities. The
437 dorsal-ventral position was determined using the border of *sna* expression.

438 **Nuclei counts.** The number of nuclei along the A-P axis was counted along the *sna* border
439 independently by two experimenters (X.C.L and L.G.), on one Z-slice where *eve* and *sna* were in
440 focus. In the posterior region where *sna* is not expressed, we counted the nuclei along the
441 extension line of the *sna* border all the way until the posterior end (excluding the pole cells). The
442 counts from the two experimenters were not significantly different. Numbers from the two
443 experimenters were averaged for each embryo. Particularly, the total number of nuclei (left panel
444 in **Fig. S4c**) were averaged across two measurements by X.C.L. and one measurement by L.G.,
445 whereas the nuclei in the most anterior and most posterior regions (middle and right panels in
446 **Fig. S4c**) were only counted once by each experimenter.

447 **Nuclei distance.** While counting the nuclei (see above), we marked the center of each nucleus
448 and extracted their x-y coordinates in ImageJ, in order to calculate the 2D-distance between
449 neighboring nuclei along the A-P axis: $D = \sqrt{(x_1 - x_2)^2 + (y_1 - y_2)^2}$, where x_1 and x_2
450 represent the x coordinates of two neighboring nuclei and y_1 and y_2 represent the y coordinates of
451 them. The average inter-nucleus distance was calculated using all nuclei counted along the A-P
452 axis and across two experimenters' measurements for each embryo (**Fig. S4d**). Additionally, we
453 plotted the inter-nucleus distance (D) as a function of the nucleus position (x_2) along the A-P axis
454 (**Fig. S4e**), which showed that the difference between F4 and F8 embryos was mainly in the
455 anterior and middle regions of the embryos.

456

457 **Cuticle preparation**

458 Overnight embryos were collected, bleached, rinsed and transferred into clean water in a
459 petri dish, where they were allowed to develop for 24h at room temperature. After 24h, the
460 larvae were transferred onto a glass slide and mounted in Hoyer's medium. The slides were
461 baked in an oven at 55°C for 48h and were then imaged with dark field microscopy.

462 The cuticle images were scored based on the criteria from Namba et al. (1997)²²: severe
463 defect – fusion or missing segments; mild defect – missing or misaligned denticles in any
464 segment; normal – no visible defects. w1118 was used as wild-type.

465

466 **Survival assay**

467 Around 100 embryos from an overnight plate were manually transferred onto an apple
468 juice plate with yeast in the center, and left at room temperature for 24h. On the second day, the
469 number of unhatched embryos were counted for each plate, and the entire agar (with larvae and
470 unhatched embryos) was transferred to a food vial. The eclosed adults were counted from day 12
471 until no adults came out. All the survival assays were performed at room temperature.

472

473 **Whole-genome sequencing**

474 *Genomic DNA extraction and library preparation*

475 We sequenced 20 F1 flies individually to estimate the level of genetic variation in the
476 founding populations (1-4 flies from each mutant pool). To prepare genomic DNA from F1
477 individuals, each fly was squished and incubated at 37 °C for 30 min in Squish Buffer (10 mM
478 Tris pH 8.0, 1 mM EDTA, 25 mM NaCl, 0.15 mg/ml Proteinase K), followed by a clean-up with
479 a Genomic DNA Clean & Concentrator kit (Zymo Research). The DNA was fragmented with a
480 customized Tn5 protocol and sequenced in 75 bp (maximum 92 bp) paired-end on an Illumina
481 NextSeq 500 at EMBL GeneCore.

482 Genomic DNA from the evolved populations was prepared using a Qiagen DNeasy
483 Tissue Kit protocol (from Alexey Veraksa), with around 100 frozen flies (about 400 ul packed
484 flies) per population. There are 38 samples: 18 populations × 2 generations (F3, F7) and 1 focal
485 population (2-6-1A) × 2 additional generations (F9, F15). They were fragmented as described

486 above and sequenced in 50 bp (maximum 88 bp) single-end on an Illumina NextSeq 2000, with a
487 pooling strategy intentionally biased toward higher coverage of 2-6-1A samples.

488 ***Read mapping and variant calling***

489 The reads were aligned to the dm6 genome with `Bowtie2`⁷³, and duplicated reads were
490 removed with `Picard` tools. To rule out Wolbachia infection, we aligned the reads to a
491 Wolbachia reference genome (wMelPop, GCF_00475015.1), and found 0.0 % of reads aligned in
492 all samples. After pre-processing, we acquired a total of 89.5 million reads for the 20 F1
493 individuals. As a preliminary analysis, we called variants in F1 individuals with `FreeBayes`⁷⁴,
494 with a threshold of 30 for mapping quality and 20 for base quality, on sites with a minimum
495 coverage of 4. We found 375,779 variable positions among F1 individuals (variant quality
496 score >10 and allele frequency < 1), suggesting a substantial amount of variation in the starting
497 populations.

498 For pooled-sequencing (Pool-seq) of evolved populations, we obtained an average of 5
499 million reads for each non-focal sample, and an average of 16 million reads for 2-6-1A samples
500 after pre-processing. Data from F1 individuals were computationally pooled. Together our reads
501 cover 36.6% of the genome. Despite the shallow coverage, we regard each read to be randomly
502 sampled from the population and the allele frequency may be roughly represented by the ratio of
503 allele depth (AD). To extract this information, we used a pipeline adapted for Pool-seq data^{34,75}:
504 first, we realigned the reads around indels and performed base recalibration with `GATK4`, using
505 the list of known variants in F1. Variable sites were then identified with `bcftools mpileup` and
506 `bcftools call`, with allele depth (AD) extracted for each sample. 936,533 positions are found
507 variable among the samples (variant quality score >10 and allele frequency < 1). The variants
508 were then annotated with `ANNOVAR`⁷⁶.

509 Unfortunately, the shallow coverage did not allow us to confidently detect EMS-induced
510 mutations in the population data. For the non-focal populations, there were 18-56 variants private
511 to each mutant pool (at sites with sufficient coverage), and there were 1,663 private variants for
512 pool 2-6, which is likely associated with the high coverage on population 2-6-1A. Therefore, we
513 focused on common variants among the populations in the genomic analysis.

514 The NGS reads are deposited at ArrayExpress (EMBL-EBI) under experiment no. E-
515 MTAB-11768.

516 ***Estimation of EMS mutation rate***

517 We used the freebayes calls from the twenty F1 individuals to estimate the mutation rate
518 induced by EMS treatment. To estimate the mutation rate, we needed to apply more stringent
519 filters to remove background mutations. We first removed indels and sites with missing data in
520 more than two individuals. Furthermore, we only kept sites with a mean depth between 4 and 50,
521 and all genotypes with a depth outside this range were considered missing data. We then used
522 `bcftools +prune` to remove small linkage blocks (sites with r^2 higher than 0.6 within a 1kb
523 window), which were likely to be background variation. After these filters, there were 13,292
524 SNPs in the dataset. We then identified SNPs that were only present in one individual (minor
525 allele count = 1), with a requirement of at least 3 reads supporting the observed allele (AO or
526 RO >2). In this way, we identified 1,036 mutations across 19 mutagenized individuals (on
527 average 55 mutations per individual) and 7 private SNPs in one non-mutagenized individual.
528 Normalized to the number of bases covered in each individual (with the same quality and depth
529 filter as when applying freebayes), the estimated mutation rate was on average 2.7 mutations per
530 Mb, ranging from 0.9 to 5.4 mutations per Mb among individuals (**Fig. S1c**). The mutation rate
531 was not obviously different between the two mutagenesis batches. Based on these data, we
532 estimated the total number of novel mutations introduced to our experimental populations to be
533 $2.7 \times 180\text{Mb} \times 3500 \text{ individuals} = 1,701,000$ mutations.

534 ***Changes in allele frequency of common variants***

535 For each population, we used `bcftools +ad-bias` to apply fisher's exact test to compare
536 allele ratio between F3 and F7, with requirements on the minimum alternative allele depth (2)
537 and minimum depth (10). Out of the 450,739 biallelic sites tested, 54,045 (12%) sites show
538 significant changes in allele frequency between generations in at least one population (FDR-
539 adjusted $p < 0.05$). The changes in allele frequency span a wide range, with most changes being
540 transitions between homozygous and heterozygous states (**Fig. S3a**), which is probably
541 associated with the detection limit imposed by sequencing depth (mean depth is 29 and median
542 depth is 21 for the sites surveyed, **Fig. S3b**).

543 Since fisher's exact test might be an overly relaxed test on allele frequency and could
544 lead to false positives^{34,77}, we applied a sign test⁷⁸ to narrow down the list of variants to those
545 showing recurrent changes in multiple populations. Each variant is given a score: $S = N_{\text{REF increase}} - N_{\text{REF decrease}}$, where $N_{\text{REF increase}}$ is the number of populations showing a significant increase in
546 reference allele frequency and $N_{\text{REF decrease}}$ is the number of populations showing a significant
547 decrease.

548 decrease in reference allele frequency. Therefore, the S score represents the tendency for the
549 alternative allele to be purged (if $S > 0$) or fixed (if $S < 0$) during evolution. Out of the 450,739
550 biallelic sites tested, 16,394 sites (4%) showed consistent increases or decreases in allele
551 frequency in more than one population. The mean of S among these sites is 0.56, suggesting a
552 slight systematic bias for detecting decreases in alternative allele frequency, but the majority of
553 the changes among populations are in random directions (mean S is close to 0). By using a cutoff
554 of $S > 5$ or $S < -5$, we report on the top 1% sites (181 among 16,394) that show consistent
555 directional changes across the parallel-evolving populations.

556 ***Genotype-phenotype association***

557 Due to the low coverage and small sample size, we used genotype calls instead of allele
558 frequency to perform genotype-phenotype association. We restricted this analysis to sites with a
559 minimum mean depth of 10, leaving 261,167 sites in the dataset. We used the mean length of F4,
560 F8, F10, and F17 embryos as the phenotype, to associate with the ‘population genotypes’ of their
561 parent generation (F3, F7, F9, and F15). Note that we used the length of F17 embryos as the
562 phenotype of F15 population, due to missing data in F16. For each variant, a linear model is used
563 to estimate the effect size and significance of the genotype. For variants with three genotypes
564 (“0/0”, “0/1” and “1/1”), the smaller p-value is used. Due to the small sample size (30 samples at
565 most), we don’t think that the association analysis has enough statistical power to support any
566 variant to be an interesting candidate, but the results could be used as a reference to prioritize
567 variants detected by the sign test (e.g. the intronic G>T mutation in *CG1136* in **Fig. S3e**). The p-
568 values are included in **Supplemental Data File 2**.

569

570 **Single-nuclei transcriptomics**

571 2.5h-to-3.5h-old embryos (developed at room temperature) were dechorionated and flash-
572 frozen in liquid nitrogen for nuclei preparation. The evolved embryos are from population 2-6-
573 1A, at the 20th generation. They were manually examined, and smaller embryos were removed
574 upon collection, to reduce noise and focus on relatively large embryos. A wild-type line (VK33)
575 and the 4 \times bcd lab stock were treated in parallel.

576 Nuclei isolation was performed following a standard protocol (10x Genomics® Single
577 Cell Protocols, with adaptations from Francisca Hervas-Sotomayor at Heidelberg University).
578 The frozen embryos were squished with a pestle for 20 times in cold homogenisation buffer

579 (HB) [250 mM sucrose, 25 mM KCl, 5 mM MgCl₂, 10 mM Tris-HCl (pH 8), 0.1% Nonidet
580 P40/IGEPAL, 1 uM DTT, 0.4 U/ul RNase Inhibitor (New England Biolabs), 0.2 U/ul
581 SUPERase•In™ RNase Inhibitor (Invitrogen)]. The samples were then centrifuged at 100 g for 1
582 min to remove unlysed tissue, and the supernatant was centrifuged at 1,000 g for 5 min to pellet
583 the nuclei. The pellet was washed once in HB, filtered twice with Flowmi® Cell Strainers
584 (Sigma), and resuspended in PBS. A subsample of the nuclei prep was DAPI-stained and
585 examined under the microscope, to determine the density of nuclei. For each sample, 7,500
586 nuclei were used as the input for 10x library construction. RNA-seq was performed on an
587 Illumina NextSeq 500 at EMBL Genomic Core Facilities (GeneCore) in two runs.

588 The reads were mapped to the *Drosophila* reference genome (dm6) plus the eGFP-Bicoid
589 plasmid sequence and counted with Cell Ranger (6.0.1), with intronic reads included. The count
590 data were analyzed with Seurat (3.9.9.9010)⁷⁹ in R, with the three samples merged into one data
591 frame. They were first filtered to remove 1) nuclei with extremely low (< 200) or high (> 4,000)
592 number of expressed genes and 2) nuclei with a high percentage of mitochondrial reads (> 5%).
593 The resulting data were normalized and scored for cell cycle status. The data were then scaled,
594 with the percentage of mitochondrial reads, percentage of ribosomal reads, and cell cycle status
595 regressed out. The scaled data were used for PCA, and Harmony⁸⁰ was used to correct for batch
596 effect, with 30 PCs. A preliminary clustering was done on the corrected data with 30 PCs and
597 three clusters with predominantly cytosolic RNA (high percentage of ribosomal and
598 mitochondrial RNA, low count in the number of genes and number of molecules) were removed.

599 After the removal, there are 3k to 6k nuclei for each sample. The data were normalized,
600 scaled, ‘harmonized’ and clustered again as described above, with 30 PCs. There are 21 clusters,
601 with no obvious cluster of doublets based on scores generated by scrublet⁸¹. Cell types were
602 inferred based on marker genes⁸², and 11 clusters were identified as early embryonic cell types
603 based on marker gene expression at stage 4-6 (*in situ* database of Berkeley Drosophila Genome
604 Project⁴⁷) (**Table S2**). Differentially expressed genes were identified with FindMarkers in
605 Seurat.

606 To curate a set of growth-related genes to examine expression changes across cell types,
607 we used the definition of insulin-like receptor signaling pathway in FlyBase (Gene group
608 FBgg0000910). Other genes were curated from Choi et al. (2015)⁸³, Welte (2015)³⁹, Heier and
609 Kühnlein (2018)⁸⁴, and Heier et al. (2021)⁸⁵.

610 The snRNA-seq reads are deposited at ArrayExpress (EMBL-EBI) under experiment no.
611 E-MTAB-12068.

612

613 **Triglycerides quantification assay**

614 The concentration of TGs in embryos was measured using the Triglyceride
615 Quantification Colorimetric Kit from Sigma (Cat. #MAK266). 50 stage5 embryos were
616 homogenized in Eppendorf tubes on a Nonidet P40 Substitute (Sigma, Cat. #74385) 5% solution.
617 The triglycerides concentration in each homogenate was then quantified following the
618 instructions provided by the manufacturer. Absorbance was measured at 570 nm.

619

620 **MALDI-imaging mass spectrometry on sectioned ovaries**

621 Ovaries needed to be cryo-sectioned to prepare the tissue for MALDI-IMS. Briefly, a
622 small number of ovaries were embedded in a previously heated 5% m/v carboxymethylcellulose
623 (Sigma) solution. This solution then solidifies at room temperature, and the resulting molds were
624 sectioned in a Leica CM1950 cryostat at -20°C, producing slices with a thickness of 20 µm.
625 These slices were then mounted on regular glass slides.

626 The samples were then coated with a microcrystalline matrix of 2,5-dihydroxybenzoic
627 acid dissolved in 70% acetonitrile to 15 mg/ml, with the help of a TM-Sprayer robotic sprayer
628 (HTX Technologies, Carrboro, NC, USA). The sprayer operated at a spray temperature of 80°C,
629 flow rate of 0.01 ml/min, track spacing of 3 mm and 10 passes, and the estimated surface
630 concentration was 3µg/mm². The glass slides were then mounted onto a custom adaptor and
631 loaded into the MS imaging ion source (AP-SMALDI5, TransMIT GmbH, Giessen, Germany).
632 Generated ions were co-axially transferred to a high mass-resolution mass spectrometer
633 (QExactive Plus mass spectrometer, ThermoFisher Scientific). Intact lipid imaging was
634 performed in positive ion mode with an isolation mass range of 400-1200. Supplementary fatty
635 acid analysis was done in negative ion mode with an isolation range of 400-1000, fragmentation
636 energy of 45 (NCE) and product isolation between 160-320.

637 Metabolite annotation was performed using the METASPACE cloud software⁸⁶ with
638 SwissLipids database⁸⁷ (version 2018-02-02). The Principal Component Analysis of these results
639 was performed on R using the FactoMineR and factoextra packages (<http://factominer.free.fr/>).
640 Enrichment analysis were carried out using LION/web⁸⁸.

641

642 **Dissection of ovarioles**

643 Flies were reared in uncrowded cages with apple juice plates supplied with yeast paste for
644 48h prior to dissection. 10-12 female flies were dissected for ovaries, which were kept on ice in
645 PBT with 4% PFA until all samples were processed. The ovaries were then fixed in PBT/PFA
646 for 30 min, washed twice in PBT and placed in Prolong Gold with DAPI. They were then further
647 dissected to separate the ovarioles and mounted on glass slides. The slides were imaged on a
648 Zeiss 880 confocal microscope and scored for ovariole number and oocyte length.

649

650 **Larval behavior**

651 Larvae (3rd instar, 5 days after egg laying) were harvested from food vials using a 10%
652 glucose solution and placed on agar plates, where their movement was recorded using a FL3-U3-
653 13Y3M-C CMOS camera (<https://www.flir.de/products/flea3-usb3/>) for two minutes. Then,
654 positional information as a function of time was automatically extracted from the videos for each
655 individual larvae using FIMtrack⁸⁹. Behavior-related parameters (speed, bending, etc) were then
656 calculated using this dataset.

657

658 **Data availability**

659 The WGS and snRNA-seq reads were deposited at ArrayExpress (EMBL-EBI) under
660 experiments E-MTAB-11768 and E-MTAB-12068, respectively. All data supporting the findings
661 of this study are available within the paper and its Supplementary Information files.

662

663 **Code availability**

664 Custom R codes and source data are deposited at: <https://git.embl.de/xuli/rapid-response-of-fly-populations-to-gene-dosage-across-development-and-generations>.

666

667 **Acknowledgements**

668 We thank Phillip Oel, Leslie Pan, Nikolaos Papadopoulos, Blanca Pijuan-Sala and Xuefei Yuan
669 for their help and advice in single-nuclei transcriptomics. We thank Ching-Ho Chang and Luisa
670 Pallares for advice on genomic analysis. We thank Dimitri Kromm and Lars Hufnagel for their
671 help in light-sheet imaging. We thank Pinar Onal and Stephen Small for sharing the Bicoid

672 antibody, and Nicolas Gompel, Artyom Kopp, and Eileen Furlong for sharing *Drosophila* stocks.
673 We also thank Martijn Molenaar for discussions on the interpretation of the metabolomics data.
674 We thank Pinar Onal and members of the Crocker group for their input on the project, in
675 particular Natalia Misunou, Mindy Liu Perkins, Albert Tsai, Rafael Galupa, Noa Otilie Borst,
676 and Gilberto Alvarez Canales for providing feedback on the manuscript. Matthew A. Benton,
677 Claire Standley and Xitong Liang also provided feedback on the manuscript. X.C.L. and L.G. are
678 supported by fellowships from the European Molecular Biology Laboratory Interdisciplinary
679 Postdoc Programme (EIPOD) under Marie Skłodowska-Curie Actions COFUND (664726 and
680 847543, respectively). Research in the Crocker lab is supported by the European Molecular
681 Biology Laboratory (EMBL).

682

683 **Author contributions**

684 Conceptualization: X.C.L, L.G., J.C. Investigation: X.C.L., L.G., M.E., K.R., J.C. Methodology:
685 X.C.L., L.G., M.E., T.A., J.C. Formal analysis: X.C.L., L.G., J.C. Data curation: X.C.L., L.G.,
686 J.C. Visualization: X.C.L., L.G., J.C. Software: X.C.L., L.G., J.C. Resources: T.A. Supervision:
687 T.A., J.C. Project administration: X.C.L., J.C. Funding acquisition: J.C. Writing, original draft:
688 X.C.L., L.G., J.C. Writing, review & editing: X.C.L., L.G., M.E., K.R., T.A., J.C.

689

690 **Competing interests**

691 The authors declare no competing interests.

692

693 **Supplementary Materials**

694 **Fig. S1.** Mutagenesis, experimental evolution and sampling scheme.

695 **Fig. S2.** Response of different populations.

696 **Fig. S3.** Changes in allele frequency in evolved populations.

697 **Fig. S4.** Embryonic phenotypes of the evolved line 2-6-1A.

698 **Fig. S5.** Single-nuclei transcriptomes of the evolved line 2-6-1A.

699 **Fig. S6.** Metabolic alterations in oocytes from the evolved line 2-6-1A.

700 **Fig. S7.** Quantification of crawling behavior of 3rd-instar larvae from 2-min videos.

701 **Fig. S8.** Cross *bicoid* transgenes into Ind and Canton-S.

702 **Fig. S9.** Ovaries in different *Drosophila* species.

703 **Table S1.** Viability of stocks carrying 2x-to-6x-*bicoid* (prior to selection).

704 **Table S2.** Marker genes and cell types for clusters in single nuclei RNA-seq.

705 **Supplemental Data File 1 (video).** Light-sheet imaging of eGFP-tagged Bicoid throughout

706 embryonic development of 4x*bcd* embryos.

707 **Supplemental Data File 2 (Microsoft Excel format).** Variants with recurrent changes across

708 multiple populations between Generation 3 and 7.

709 **Supplemental Data File 3 (Microsoft Excel format).** Marker genes of yolk cluster that are

710 differentially expressed in the evolved line.

711 **Supplemental Data File 4 (Microsoft Excel format).** Differentially expressed genes between

712 the evolved line and the other two samples.

713 **Supplemental Data File 5 (Microsoft Word format).** Map of eGFP-Bicoid construct used to

714 generate the 4x*bcd* line in this study.

715

716 **Reference**

717 1. Wittkopp, P. J. & Kalay, G. Cis-regulatory elements: molecular mechanisms and

718 evolutionary processes underlying divergence. *Nat. Rev. Genet.* **13**, 59–69 (2012).

719 2. Fuqua, T. *et al.* Dense and pleiotropic regulatory information in a developmental enhancer.

720 *Nature* **587**, 235–239 (2020).

721 3. Davies, J. Using synthetic biology to explore principles of development. *Dev. Camb.* **144**,

722 1146–1158 (2017).

723 4. Davidson, E. H. *The Regulatory Genome: Gene Regulatory Networks In Development And*

724 *Evolution - Eric H. Davidson - Google Books. The Regulatory Genome: Gene Regulatory*

725 *Networks In Development And Evolution* (Academic Press, 2010).

726 5. Miyazawa, H. & Aulehla, A. Revisiting the role of metabolism during development.

727 *Development* **145**, (2018).

728 6. Gilbert, S. F., Bosch, T. C. G. & Ledón-Rettig, C. Eco-Evo-Devo: developmental symbiosis

729 and developmental plasticity as evolutionary agents. *Nat. Rev. Genet.* **16**, 611–622 (2015).

730 7. Bergelson, J., Kreitman, M., Petrov, D. A., Sanchez, A. & Tikhonov, M. Functional biology
731 in its natural context: a search for emergent simplicity. *eLife* **10**, 1–12 (2021).

732 8. Weber, M. *Philosophy of Developmental Biology*. (Cambridge University Press, Cambridge,
733 2022). doi:10.1017/9781108954181.

734 9. Jacob, F. *The Possible and the Actual*. (University of Washington Press, 1982).

735 10. Boyle, E. A., Li, Y. I. & Pritchard, J. K. An Expanded View of Complex Traits: From
736 Polygenic to Omnipotent. *Cell* **169**, 1177–1186 (2017).

737 11. Frankel, N. *et al.* Morphological evolution caused by many subtle-effect substitutions in
738 regulatory DNA. *Nature* **474**, 598–603 (2011).

739 12. Wood, A. R. *et al.* Defining the role of common variation in the genomic and biological
740 architecture of adult human height. *Nat. Genet.* **46**, 1173 (2014).

741 13. Yengo, L. *et al.* Meta-analysis of genome-wide association studies for height and body mass
742 index in ~700000 individuals of European ancestry. *Hum. Mol. Genet.* **27**, 3641–3649
743 (2018).

744 14. Houle, D., Govindaraju, D. R. & Omholt, S. Phenomics: the next challenge. *Nat. Rev. Genet.*
745 **11**, 855–866 (2010).

746 15. Perkins, M. L., Gandara, L. & Crocker, J. A synthetic synthesis to explore animal evolution
747 and development. *Philos. Trans. R. Soc. B Biol. Sci.* **377**, 20200517 (2022).

748 16. Gandara, L. *et al.* Developmental phenomics suggests that H3K4 monomethylation confers
749 multi-level phenotypic robustness. *Cell Rep.* **41**, (2022).

750 17. Nüsslein-Volhard, C. & Wieschaus, E. Mutations affecting segment number and polarity in
751 *Drosophila*. *Nature* **287**, 795–801 (1980).

752 18. Briscoe, J. & Small, S. Morphogen rules: design principles of gradient-mediated embryo
753 patterning. *Development* **142**, 3996–4009 (2015).

754 19. Driever, W. & Nüsslein-Volhard, C. The bicoid protein determines position in the
755 Drosophila embryo in a concentration-dependent manner. *Cell* **54**, 95–104 (1988).

756 20. Houchmandzadeh, B., Wieschaus, E. & Leibler, S. Establishment of developmental precision
757 and proportions in the early Drosophila embryo. *Nature* **415**, 798–802 (2002).

758 21. Gregor, T., Bialek, W., De Ruyter Van Steveninck, R. R., Tank, D. W. & Wieschaus, E. F.
759 Diffusion and scaling during early embryonic pattern formation. *Proc. Natl. Acad. Sci. U. S.
760 A.* **102**, 18403–18407 (2005).

761 22. Namba, R., Pazdera, T. M., Cerrone, R. L. & Minden, J. S. Drosophila embryonic pattern
762 repair: How embryos respond to bicoid dosage alteration. *Development* **124**, 1393–1403
763 (1997).

764 23. Berleth, T. *et al.* The role of localization of bicoid RNA in organizing the anterior pattern of
765 the Drosophila embryo. *EMBO J.* **7**, 1749–56 (1988).

766 24. Lott, S. E., Kreitman, M., Palsson, A., Alekseeva, E. & Ludwig, M. Z. Canalization of
767 segmentation and its evolution in Drosophila. *Proc. Natl. Acad. Sci.* **104**, 10926–10931
768 (2007).

769 25. Teleman, A. A., Chen, Y. W. & Cohen, S. M. Drosophila melted modulates FOXO and TOR
770 activity. *Dev. Cell* **9**, 271–281 (2005).

771 26. Lobell, A. S., Kaspari, R. R., Serrano Negron, Y. L. & Harbison, S. T. The genetic
772 architecture of Ovariole number in Drosophila melanogaster: Genes with major, quantitative,
773 and pleiotropic effects. *G3 Genes Genomes Genet.* **7**, 2391–2403 (2017).

774 27. Busturia, A. & Lawrence, P. A. Regulation of cell number in *Drosophila*. *Nature* **370**, 561–
775 563 (1994).

776 28. Lenski, R. E. Experimental evolution and the dynamics of adaptation and genome evolution
777 in microbial populations. *ISME J.* **11**, 2181–2194 (2017).

778 29. Good, B. H., McDonald, M. J., Barrick, J. E., Lenski, R. E. & Desai, M. M. The dynamics of
779 molecular evolution over 60,000 generations. *Nature* **551**, 45–50 (2017).

780 30. Levy, S. F. *et al.* Quantitative evolutionary dynamics using high-resolution lineage tracking.
781 *Nature* **519**, 181–186 (2015).

782 31. Moulana, A. *et al.* Compensatory epistasis maintains ACE2 affinity in SARS-CoV-2
783 Omicron BA.1. *Nat. Commun.* **13**, 7011 (2022).

784 32. Huang, A., Rupprecht, J.-F. & Saunders, T. E. Embryonic geometry underlies phenotypic
785 variation in decanalized conditions. *eLife* **9**, 1–21 (2020).

786 33. Miles, C. M. *et al.* ARTIFICIAL SELECTION ON EGG SIZE PERTURBS EARLY
787 PATTERN FORMATION IN DROSOPHILA MELANOGASTER. *Evolution* **65**, 33–42
788 (2011).

789 34. Jha, A. R. *et al.* Whole-genome resequencing of experimental populations reveals polygenic
790 basis of egg-size variation in *drosophila melanogaster*. *Mol. Biol. Evol.* **32**, 2616–2632
791 (2015).

792 35. Azevedo, R. B. R., French, V. & Partridge, L. Thermal Evolution of Egg Size in *Drosophila*
793 *melanogaster*. *Evolution* **50**, 2338 (1996).

794 36. Church, S. H., Donoughe, S., de Medeiros, B. A. S. & Extavour, C. G. Insect egg size and
795 shape evolve with ecology but not developmental rate. *Nature* **571**, 58–62 (2019).

796 37. Böhni, R. *et al.* Autonomous Control of Cell and Organ Size by CHICO, a Drosophila
797 Homolog of Vertebrate IRS1–4. *Cell* **97**, 865–875 (1999).

798 38. Oldham, S. *et al.* The Drosophila insulin/IGF receptor controls growth and size by
799 modulating PtdInsP3 levels. *Development* **129**, 4103–4109 (2002).

800 39. Welte, M. A. As the fat flies: The dynamic lipid droplets of Drosophila embryos. *Biochim.*
801 *Biophys. Acta BBA - Mol. Cell Biol. Lipids* **1851**, 1156–1185 (2015).

802 40. Tennessen, J. M. *et al.* Coordinated Metabolic Transitions During Drosophila
803 Embryogenesis and the Onset of Aerobic Glycolysis. *G3 GenesGenomesGenetics* **4**, 839–
804 850 (2014).

805 41. Němec, V. Quantitative changes in protein, glycogen and fat content in the eggs of the
806 locusts, *Locusta migratoria migratorioides* and *Schistocerca gregaria* (Orthoptera), during
807 embryogenesis. *Eur. J. Entomol.* **99**, 557–559 (2002).

808 42. Mensch, J., Di Battista, C., De Majo, M. S., Campos, R. E. & Fischer, S. Increased size and
809 energy reserves in diapausing eggs of temperate *Aedes aegypti* populations. *J. Insect*
810 *Physiol.* **131**, (2021).

811 43. Caprioli, R. M., Farmer, T. B. & Gile, J. Molecular imaging of biological samples:
812 localization of peptides and proteins using MALDI-TOF MS. *Anal. Chem.* **69**, 4751–4760
813 (1997).

814 44. He, F. *et al.* Fundamental origins and limits for scaling a maternal morphogen gradient. *Nat.*
815 *Commun.* **6**, 6679 (2015).

816 45. Church, S. H., de Medeiros, B. A. S., Donoughe, S., Márquez Reyes, N. L. & Extavour, C.
817 G. Repeated loss of variation in insect ovary morphology highlights the role of development
818 in life-history evolution. *Proc. R. Soc. B Biol. Sci.* **288**, 20210150 (2021).

819 46. Green, D. A. Developmental and Genetic Mechanisms of Ovariole Number Evolution in
820 Drosophila. (Harvard University, 2014).

821 47. Hammonds, A. S. *et al.* Spatial expression of transcription factors in Drosophilaembryonic
822 organ development. *Genome Biol.* **14**, R140 (2013).

823 48. Cheung, D., Miles, C., Kreitman, M. & Ma, J. Adaptation of the length scale and amplitude
824 of the Bicoid gradient profile to achieve robust patterning in abnormally large Drosophila
825 melanogaster embryos. *Development* **141**, 124–135 (2014).

826 49. He, F. *et al.* Probing Intrinsic Properties of a Robust Morphogen Gradient in Drosophila.
827 *Dev. Cell* **15**, 558–567 (2008).

828 50. Cheung, D., Miles, C., Kreitman, M. & Ma, J. Scaling of the Bicoid morphogen gradient by
829 a volume-dependent production rate. *Development* **138**, 2741–2749 (2011).

830 51. Rudman, S. M. *et al.* Direct observation of adaptive tracking on ecological time scales in
831 Drosophila. *Science* **375**, (2022).

832 52. Suvorov, A. *et al.* Widespread introgression across a phylogeny of 155 Drosophila genomes.
833 *Curr. Biol.* **32**, 111-123.e5 (2022).

834 53. Liu, X., Li, Y. I. & Pritchard, J. K. Trans Effects on Gene Expression Can Drive Omnipotent
835 Inheritance. *Cell* **177**, 1022-1034.e6 (2019).

836 54. Bothma, J. P. *et al.* Dynamic regulation of eve stripe 2 expression reveals transcriptional
837 bursts in living Drosophila embryos. *Proc. Natl. Acad. Sci. U. S. A.* **111**, 10598–603 (2014).

838 55. Cheung, D. & Ma, J. Probing the impact of temperature on molecular events in a
839 developmental system. *Sci. Rep.* **5**, 13124 (2015).

840 56. Clark, E., Battistara, M. & Benton, M. A. A timer gene network is spatially regulated by the
841 terminal system in the Drosophila embryo. *eLife* **11**, 2022.01.26.477848 (2022).

842 57. Liu, F., Morrison, A. H. & Gregor, T. Dynamic interpretation of maternal inputs by the
843 Drosophila segmentation gene network. *Proc. Natl. Acad. Sci.* **110**, 6724–6729 (2013).

844 58. Nikolić, M. *et al.* Scale invariance in early embryonic development. Preprint at
845 <http://arxiv.org/abs/2312.17684> (2023).

846 59. Holloway, D. M., Harrison, L. G., Kosman, D., Vanario-Alonso, C. E. & Spirov, A. V.
847 Analysis of Pattern Precision Shows That Drosophila Segmentation Develops Substantial
848 Independence From Gradients of Maternal Gene Products. *Dev. Dyn.* **235**, 2949 (2006).

849 60. Petkova, M. D., Tkačik, G., Bialek, W., Wieschaus, E. F. & Gregor, T. Optimal Decoding of
850 Cellular Identities in a Genetic Network. *Cell* **176**, 844-855.e15 (2019).

851 61. Rockman, M. V. The QTN Program and the Alleles That Matter for Evolution: All That's
852 Gold Does Not Glitter. *Evolution* **66**, 1–17 (2012).

853 62. Zhang, W., Reeves, G. R. & Tautz, D. Testing Implications of the Omnigenic Model for the
854 Genetic Analysis of Loci Identified through Genome-wide Association. *Curr. Biol.* **31**, 1092–
855 1098.e6 (2021).

856 63. Moczek, A. P. *et al.* The role of developmental plasticity in evolutionary innovation. *Proc.*
857 *R. Soc. B Biol. Sci.* **278**, 2705–2713 (2011).

858 64. Fuqua, T. *et al.* An open-source semi-automated robotics pipeline for embryo
859 immunohistochemistry. *Sci. Rep.* **11**, 1–16 (2021).

860 65. Keightley, P. D. Nature of Deleterious Mutation Load in Drosophila. *Genetics* **144**, 1993–
861 1999 (1996).

862 66. Schaid, D. J., Chen, W. & Larson, N. B. From genome-wide associations to candidate causal
863 variants by statistical fine-mapping. *Nat. Rev. Genet.* **19**, 491–504 (2018).

864 67. White, C. R., Alton, L. A., Bywater, C. L., Lombardi, E. J. & Marshall, D. J. Metabolic
865 scaling is the product of life-history optimization. *Science* **377**, 834–839 (2022).

866 68. Gregor, T., Wieschaus, E. F., McGregor, A. P., Bialek, W. & Tank, D. W. Stability and
867 Nuclear Dynamics of the Bicoid Morphogen Gradient. *Cell* **130**, 141–152 (2007).

868 69. Bökel, C. EMS Screens. in *Methods in molecular biology* (Clifton, N.J.) vol. 420 119–138
869 (2008).

870 70. Galupa, R. *et al.* Enhancer architecture and chromatin accessibility constrain phenotypic
871 space during development. *bioRxiv* **38**, 2022.06.02.494376 (2022).

872 71. Dubuis, J. O., Samanta, R. & Gregor, T. Accurate measurements of dynamics and
873 reproducibility in small genetic networks. *Mol. Syst. Biol.* **9**, 639 (2013).

874 72. Crocker, J., Ilsley, G. R. & Stern, D. L. Quantitatively predictable control of Drosophila
875 transcriptional enhancers in vivo with engineered transcription factors. *Nat. Genet.* **48**, 292–
876 298 (2016).

877 73. Langmead, B. & Salzberg, S. L. Fast gapped-read alignment with Bowtie 2. *Nat Methods* **9**,
878 357–359 (2012).

879 74. Garrison, E. & Marth, G. Haplotype-based variant detection from short-read sequencing.
880 *arXiv* 1207.3907 (2012) doi:10.48550/arxiv.1207.3907.

881 75. Schlötterer, C., Tobler, R., Kofler, R. & Nolte, V. Sequencing pools of individuals-mining
882 genome-wide polymorphism data without big funding. *Nat. Rev. Genet.* **15**, 749–763 (2014).

883 76. Wang, K., Li, M. & Hakonarson, H. ANNOVAR: functional annotation of genetic variants
884 from high-throughput sequencing data. *Nucleic Acids Res.* **38**, e164–e164 (2010).

885 77. Turner, T. L., Stewart, A. D., Fields, A. T., Rice, W. R. & Tarone, A. M. Population-based
886 resequencing of experimentally evolved populations reveals the genetic basis of body size
887 variation in *Drosophila melanogaster*. *PLoS Genet.* **7**, (2011).

888 78. Orr, H. The population genetics of adaptation: the distribution of factors fixed during
889 adaptive evolution. *Evolution* **52**, 935–949 (1998).

890 79. Stuart, T. *et al.* Comprehensive Integration of Single-Cell Data. *Cell* **177**, 1888-1902.e21
891 (2019).

892 80. Korsunsky, I. *et al.* Fast, sensitive and accurate integration of single-cell data with Harmony.
893 *Nat. Methods* **16**, 1289–1296 (2019).

894 81. Wolock, S. L., Lopez, R. & Klein, A. M. Scrublet: Computational Identification of Cell
895 Doublets in Single-Cell Transcriptomic Data. *Cell Syst.* **8**, 281-291.e9 (2019).

896 82. Karaïkos, N. *et al.* The *Drosophila* embryo at single-cell transcriptome resolution. *Science*
897 **358**, 194–199 (2017).

898 83. Choi, S., Lim, D.-S. & Chung, J. Feeding and Fasting Signals Converge on the LKB1-SIK3
899 Pathway to Regulate Lipid Metabolism in *Drosophila*. *PLOS Genet.* **11**, e1005263 (2015).

900 84. Heier, C. & Kühnlein, R. P. Triacylglycerol metabolism in *drosophila melanogaster*.
901 *Genetics* **210**, 1163–1184 (2018).

902 85. Heier, C., Klishch, S., Stilbytska, O., Semaiuk, U. & Lushchak, O. The *Drosophila* model to
903 interrogate triacylglycerol biology. *Biochim. Biophys. Acta - Mol. Cell Biol. Lipids* **1866**,
904 158924 (2021).

905 86. Alexandrov, T. *et al.* METASPACE: A community-populated knowledge base of spatial
906 metabolomes in health and disease. *bioRxiv* 539478 (2019) doi:10.1101/539478.

907 87. Aimo, L. *et al.* The SwissLipids knowledgebase for lipid biology. *Bioinformatics* **31**, 2860–
908 2866 (2015).

909 88. Molenaar, M. R. *et al.* LION/web: a web-based ontology enrichment tool for lipidomic data
910 analysis. *GigaScience* **8**, giz061 (2019).

911 89. Risse, B., Berh, D., Otto, N., Klämbt, C. & Jiang, X. FIMTrack: An open source tracking
912 and locomotion analysis software for small animals. *PLOS Comput. Biol.* **13**, e1005530
913 (2017).

914